

CONSTRAINING THE SPIN-DOWN OF THE NEARBY ISOLATED NEUTRON STAR RX J0806.4–4123, AND IMPLICATIONS FOR THE POPULATION OF NEARBY NEUTRON STARS

D. L. KAPLAN¹ AND M. H. VAN KERKWIJK²

Accepted for publication in ApJ

ABSTRACT

The nearby isolated neutron stars are a group of seven relatively slowly rotating neutron stars that show thermal X-ray spectra, most with broad absorption features. They are interesting both because they may allow one to determine fundamental neutron-star properties by modeling their spectra, and because they appear to be a large fraction of the overall neutron-star population. Here, we describe a series of *XMM-Newton* observations of the nearby isolated neutron star RX J0806.4–4123, taken as part of larger program of timing studies. From these, we limit the spin-down rate to $\dot{\nu} = (-4.3 \pm 2.3) \times 10^{-16} \text{ Hz s}^{-1}$. This constrains the dipole magnetic field to be $< 3.7 \times 10^{13} \text{ G}$ at 2σ , significantly less than the field of $\sim 10^{14} \text{ G}$ implied by simple models for the X-ray absorption found at 0.45 keV. We confirm that the spectrum is thermal and stable (to within a few percent), but find that the 0.45 keV absorption feature is broader and more complex than previously thought. Considering the population of isolated neutron stars, we find that magnetic field decay from an initial field of $\lesssim 3 \times 10^{14} \text{ G}$ accounts most naturally for their timing and spectral properties, both qualitatively and in the context of the models for field decay of Pons and collaborators.

Subject headings: magnetic fields — stars: individual (RX J0806.4-4123) — stars: neutron — X-rays: stars

1. INTRODUCTION

The so-called isolated neutron stars (INS; see Haberl 2007 and Kaplan 2008 for reviews) are a group of seven (confirmed) nearby ($\lesssim 1 \text{ kpc}$) neutron stars with low ($\sim 10^{32} \text{ erg s}^{-1}$) X-ray luminosities and long (3–11 s) spin periods. They stand out from the normal neutron star population because of their timing properties (which should not have influenced their method of discovery via soft X-ray emission, although see Heyl & Kulkarni 1998). The X-ray luminosities are consistent with cooling neutron stars of ages $\sim 0.5 \text{ Myr}$ (Page et al. 2004), in rough agreement with their kinematic ages (Walter 2001; Kaplan, van Kerkwijk, & Anderson 2002c; Motch et al. 2005; Kaplan et al. 2007; Motch et al. 2009).

A crucial unknown in understanding the INS is their magnetic field strengths. This is important in understanding the X-ray spectra (Zane, Turolla, & Drake 2004; Motch, Zavlin, & Haberl 2003; Ho et al. 2007; van Kerkwijk & Kaplan 2007; Haberl 2007) and their thermal history (Heyl & Kulkarni 1998). The X-ray spectra of the INS appear thermal, with temperatures of $\sim 10^6 \text{ K}$ and with, in all but one source, broad absorption features at energies of 0.2 to 0.75 keV. These features may give clues to the chemical composition and structure of the INS surfaces, but also depend strongly on the magnetic field. For a hydrogen atmosphere the simplest possibilities are electron and proton cyclotron resonances or transitions between bound states of neutral hydrogen, all of which depend on the field strength. Even with different compositions (or states) the field strength is still relevant. At the same time, the magnetic field can affect

the cooling rate and thermal content of the neutron star atmosphere (e.g., Pons, Miralles, & Geppert 2009, and references therein).

Dipolar magnetic field strengths can be estimated from coherent timing solutions, and we used X-ray observations to derive such solutions for four INS, finding magnetic fields of $(1 - 3) \times 10^{13} \text{ G}$ (Kaplan & van Kerkwijk 2005a,b; van Kerkwijk & Kaplan 2008; Kaplan & van Kerkwijk 2009, hereafter KvK05a,b, vKK08, KvK09; also see van Kerkwijk et al. 2007). Here, we constrain the spin-down rate and hence magnetic field strength of the INS RX J0806.4–4123 (hereafter RX J0806) with a series of dedicated *XMM-Newton* observations. We also present a preliminary spectral analysis, but defer a detailed phase-resolved analysis to a later paper.

RX J0806 was identified as a possible neutron star by Haberl, Motch, & Pietsch (1998) on the basis of a soft thermal spectrum and the absence of an optical counterpart. Using *XMM*, Haberl & Zavlin (2002) confirmed that the spectrum was soft and blackbody-like and identified a candidate 11.37 s periodicity. Further observations confirmed this periodicity and also suggested that the X-ray spectrum was not purely a blackbody, but had a broad absorption feature at $\approx 0.45 \text{ keV}$ (Haberl et al. 2004b; hereafter H+04). In what follows, we assume a distance of 250 pc to RX J0806, derived by Posselt et al. (2007) from a comparison of the X-ray absorption column density with a model for the interstellar medium (using $N_{\text{H}} = 1.0 \times 10^{20} \text{ cm}^{-2}$, consistent with what we infer).

With RX J0806, we now have spin-down measurements or constraints for five of the seven confirmed INS. Examining the global properties of the INS relative to other related neutron star populations, we attempt to understand how the INS fit with the other groups.

¹ Hubble Fellow; KITP, Kohn Hall, University of California, Santa Barbara, CA 93106; dkaplan@kitp.ucsb.edu

² Department of Astronomy and Astrophysics, University of Toronto, 50 St. George Street, Toronto, ON M5S 3H4, Canada; mhvk@astro.utoronto.ca

TABLE 1
LOG OF OBSERVATIONS AND TIMES OF ARRIVAL

Rev.	Date	Exp. ^a (ks)	Counts ^a	f_{bg} ^a (%)	TOA ^b (MJD)
168	2000 Nov 08	15.6	25,604	1.6	51856.691599(3)
618	2003 Apr 24	22.0	37,300	1.5	52753.747077(3)
1542	2008 May 11	9.0	11,467	4.1	54597.501552(4)
1544	2008 May 15	10.0	12,590	4.4	54601.309174(4)
1551	2008 May 29	5.0	7,107	4.8	54615.274494(6)
1562	2008 Jun 20	13.0	18,016	9.2	54637.594919(5)
1621	2008 Oct 15	9.0	12,224	4.2	54754.488408(4)
1631	2008 Nov 04	5.0	7,272	4.7	54774.185892(8)
1633	2008 Nov 09	6.0	9,386	27.8	54779.285979(6)
1649	2008 Dec 10	9.0	12,427	4.4	54810.460578(4)
1705	2009 Mar 31	9.0	11,185	4.6	54921.908923(4)
1705	2009 Apr 01	26.0	41,755	23.7	54922.901462(4)
1710	2009 Apr 11	8.0	11,027	5.8	54932.057781(4)

NOTE. — All observations used the small window mode and thin filter for both EPIC-pn and EPIC-MOS1/2, except for Revs. 168 and 618, in which the full window mode was used, which meant that only the EPIC-pn data were suitable for timing.

^a The exposure time, number of counts, and estimated fraction of events due to background f_{bg} given here are for EPIC-pn only.

^b The TOA is defined as the time of maximum light of the fundamental (following Eqn. 1) closest to the middle of each observation computed from the combined EPIC-pn and EPIC-MOS1/2 datasets, and is given with 1- σ uncertainties.

The structure of this paper is as follows. In Section 2, we present our new data and perform our timing (§ 2.1) and spectroscopic (§ 2.2) analyses. We then consider the implications of these results. In § 3.1, we compare the timing and spectral properties of RX J0806 to the rest of the INS and try to understand the origin of the X-ray absorption features. In § 3.2, we extend the comparison to the pulsar population as a whole, exploring the qualitative relation between the INS and relevant sub-populations of pulsars. From this, we are led to consider the role that magnetic field decay may play in the evolution of the INS, and in § 3.3 we discuss our results in the context of a specific model for field decay, that of Pons et al. (2009). Finally, we conclude in § 4.

2. OBSERVATIONS & ANALYSIS

We observed RX J0806 eleven times with *XMM* (Jansen et al. 2001) in 2008 and 2009, and focus here on the data taken with the European Photon Imaging Camera (EPIC) with pn and MOS detectors, all used in small window mode with thin filters (Table 1). All our observations, as well as those from Haberl & Zavlin (2002) and H+04 (taken with the same filter, but with the full window mode instead), were processed with SAS version 8.0.1. We used `epchain` and `emchain` and selected source events from a circular region of $37''.5$ radius with energies between 150 eV (the default) and 1.2 keV (where flares are minimized; the source is not detected above 1.2 keV, and the background grows increasingly dominant below 150 eV). As recommended, we included only one and two-pixel (single and double patterns 0–4) events with no warning flags for pn, and single, double, and triple events (patterns 0–12) with the default flag mask for MOS1/2. We barycentered the event times using the *Chandra X-ray Observatory* position from H+04: $\alpha = 08^h06^m23^s.40$ and $\delta = -41^\circ22'30''.9$ (J2000). We extracted background lightcurves for pn from similarly

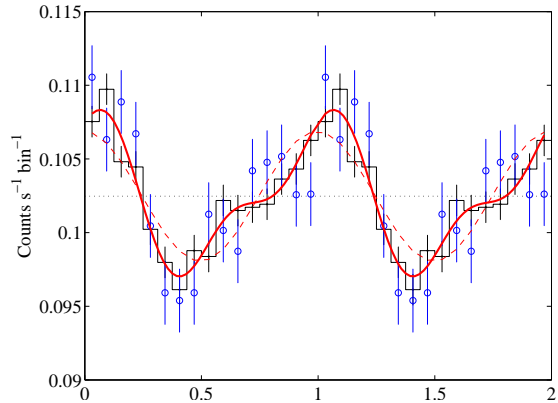


FIG. 1.— Pulse profile of RX J0806, repeated twice for clarity. We show the background-subtracted EPIC count-rate in each of 16 bins as a function of pulse phase. The solid curve is the best-fit model including the first harmonic, while for comparison we also draw the best-fit sinusoid as the dashed curve. The histogram/points include all events from our 2008–2009 observations phased up following Table 2, while the open circles are the longest single observation (Rev. 618 from 2003).

sized regions offset from the source, but at the same RAWY coordinate, as recommended by the SAS User Guide.³ For MOS1/2, the small-window mode does not permit such large background areas, but we used several smaller areas to compensate. The background rate for our data (up to $\sim 24\%$ in one case) was higher than for the archival data ($\sim 2\%$), in some cases due to severe flares. However, restricting the time ranges to remove the flares did not significantly alter our results or precision.

2.1. Timing Analysis

As a starting place, we first determined the frequency that maximized the power in a Z_1^2 periodogram for the EPIC-pn data from Rev. 1562 (the observation in 2008–2009 with the highest Z_1^2 power). We found a best-fit frequency of $\nu = 0.087958 \pm 0.000006$ Hz, consistent with that found by H+04 for the earlier data. A Z_2^2 periodogram that incorporates the first harmonic (see below) gives the same result with slightly better precision, where the uncertainty on ν is found with the same analytic expression as for the Z_1^2 result (based on Ransom, Eikenberry, & Middleditch 2002) and we have verified with simulations that this is correct.

Using the above frequency, we determined the times-of-arrival (TOAs; see Table 1) for the combined EPIC data from each observation by fitting the binned lightcurves (following KvK05b; we verified that we obtained similar results from unbinned fits following Cash 1979). Like Haberl & Zavlin (2002), we found that the lightcurve of RX J0806 was best described not by a single sinusoid but instead by a sinusoid and its first harmonic, where the number of counts in bin i are:

$$N_i = A \{ \cos [2\pi(f_0 t_i - \phi_0)] + r_2 \cos [4\pi(f_0 t_i - \phi_0 - \Delta\phi_2)] \} + C \quad (1)$$

where f_0 is the frequency of the fundamental from above, t_i is the time of bin i on the interval $[0, 1/f_0)$, and the fit parameters are amplitude A , phase ϕ_0 , amplitude ratio r_2 , phase offset $\Delta\phi_2$, and constant rate C , similar to KvK05b. We found initial best-fit parameters from the

³ See http://xmm.esac.esa.int/external/xmm_user_support/documentation

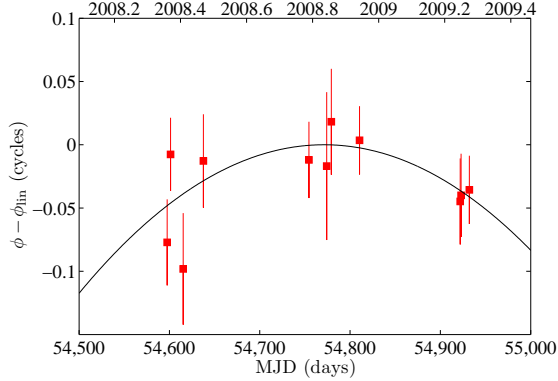


FIG. 2.— Phase residuals for RX J0806. We show the residuals relative to a linear model ($\dot{\nu} = 0$). The line shows the best-fit quadratic solution.

longer observations, finding that all were reasonably consistent with a constant pulse profile with $A/C \approx 4.6\%$, $r_2 \approx 0.45$, and $\Delta\phi_2 \approx 0.11$ (corrected for background). This is consistent with the $\sim 6\%$ pulsed fraction found by H+04. We refined the parameters using the combined event list derived from all 2008–2009 observations phased together (see below).

The spacing and precision of the TOAs is insufficient for an unambiguous timing solution (unlike in KvK05a,b but like in vKK08 and KvK09). Instead we searched for possible coherent timing solutions by iteratively trying sets of cycle counts between the different TOAs from 2008 and 2009 (similar to vKK08, although as with KvK09 we did not incorporate frequency information from each observation because it does not add extra information). We limit solutions to $|\dot{\nu}| \lesssim 1.5 \times 10^{-13} \text{ Hz s}^{-1}$, the $3\text{-}\sigma$ incoherent limit from H+04.

We find one solution that is considerably better than the alternatives with $\chi^2 = 5.1$ for 8 degrees of freedom (DOF) and a small, not-quite significant spin-down rate of $\dot{\nu} = (-4.3 \pm 2.3) \times 10^{-16} \text{ Hz s}^{-1}$ (see Fig. 2, Table 2). This gives a 2σ limit on the magnetic field of field of $B_{\text{dip}} < 3.7 \times 10^{13} \text{ G}$. The next best solution has $\chi^2 = 27.2$ and a very different spin-down rate: $(+4.32 \pm 0.02) \times 10^{-14} \text{ Hz s}^{-1}$. For a fit with 3 free parameters, a change in χ^2 of 22.1 means that the best-fit solution is favored at 99.994% confidence. Even less likely solutions are found for combinations of other cycle counts.

We confirmed this solution using a coherent Z_1^2 periodogram as a function of both ν and $\dot{\nu}$. The best solution was consistent with that found in the TOA analysis, although it varied by $\sim 1\sigma$ in $\dot{\nu}$. This is likely because the Z_1^2 did not incorporate any information about the harmonic, while the TOA analysis did. The best-fit peak has $Z_1^2 = 162.3$, consistent with the background-corrected rms pulsed fraction of $\approx 3.8\%$. Spin-down is not detected with $Z_1^2(\dot{\nu} = 0) = 162.2$, as the Z_1^2 does not include the harmonic. Including the harmonic at arbitrary phase and amplitude we get $Z_2^2 = 206.9$ at $(\nu, \dot{\nu}) = (0.0879477628 \pm 8 \times 10^{-10} \text{ Hz}, (-2.0 \pm 3.6) \times 10^{-16} \text{ Hz s}^{-1})$, very close to the location of the coherent solution (the increased uncertainty comes from not including constraints on the pulse profile).

After performing our coherent timing solution, we

TABLE 2
MEASURED AND DERIVED TIMING
PARAMETERS FOR RX J0806.4–4123

Quantity	Value
Dates (MJD) ..	54,598–54,932
t_0 (MJD).....	54771.319605(2)
ν (Hz)	0.0879477624(9)
$\dot{\nu}$ ($10^{-16} \text{ Hz s}^{-1}$)	−4.3(23)
TOA rms (s) ...	0.4
χ^2/DOF	5.1/8
P (s).....	11.37038592(12)
\dot{P} ($10^{-14} \text{ s s}^{-1}$)..	5.5(30)
τ_{char} (Myr).....	3.3
B_{dip} (10^{13} G) ..	2.5
\dot{E} ($10^{30} \text{ erg s}^{-1}$)	1.5

NOTE. — Quantities in parentheses are the formal $1\text{-}\sigma$ uncertainties on the last digit. $\tau_{\text{char}} = P/2\dot{P}$ is the characteristic age, assuming an initial spin period $P_0 \ll P$ and a constant magnetic field; $B_{\text{dip}} = 3.2 \times 10^{19} \sqrt{P\dot{P}} \text{ G}$ is the magnetic field inferred assuming spin-down by dipole radiation; $\dot{E} = 3.9 \times 10^{46} \nu \dot{\nu} \text{ erg s}^{-1}$ is the spin-down luminosity. In addition to the nominal values above, the $2\text{-}\sigma$ limits to those quantities (based on $\dot{\nu} > -8.9 \times 10^{-16} \text{ Hz s}^{-1}$) are $\tau_{\text{char}} > 1.5 \text{ Myr}$, $B_{\text{dip}} < 3.7 \times 10^{13} \text{ G}$, and $\dot{E} < 2.8 \times 10^{30} \text{ erg s}^{-1}$.

made a pulse profile using the events from all 2008–2009 observations (Fig. 1). We found that the shape was consistent with what we had assumed above, but that changing the pulse shape parameters within the measured uncertainties changed the timing solution slightly, typically by 10% in $\dot{\nu}$ (20% of the uncertainty on $\dot{\nu}$). Similarly, changing the timing solution within the uncertainties changed the fitted parameters slightly. However, since all such changes were significantly less than the uncertainties, we decided to choose an average set of pulse profile parameters and use them throughout. The final parameters that we used were $A/C = 0.046 \pm 0.004$, $r_2 = 0.45 \pm 0.10$, and $\Delta\phi_2 = 0.11 \pm 0.02$ (i.e., our arrival times are based on fits in which only ϕ_0 and C are free parameters). These values are consistent with the timing solution given above and in Table 2. The profile with the harmonic is preferred greatly to just a sinusoid, with $\chi^2 = 43.8$ for 13 DOF (fundamental only) vs. $\chi^2 = 14.2$ for 11 DOF (with the harmonic). Changing parameters slightly gives similar but slightly different results. For example, with $r_2 = 0.55$ instead of 0.45, we find $\dot{\nu}$ decreases by 2% which is 5% of the uncertainty on $\dot{\nu}$. Decreasing A/C to 4% increases $\dot{\nu}$ by 7% (15% of the uncertainty on $\dot{\nu}$). The energy range that we used also affects our results slightly, but the solution remains consistent overall. For instance, we see slight differences if we restrict our analysis to the energy range of 300–500 eV, where the pulsations from RX J0806 are the very strong and the spectrum shows X-ray absorption (see below). While the pulsation amplitude increases to $A/C = 7\%$, the timing solution is consistent with $\dot{\nu} = (-2.1 \pm 2.2) \times 10^{-16} \text{ Hz s}^{-1}$.

Unfortunately, we cannot unambiguously extrapolate our solution back to the 2000 and 2003 observations and

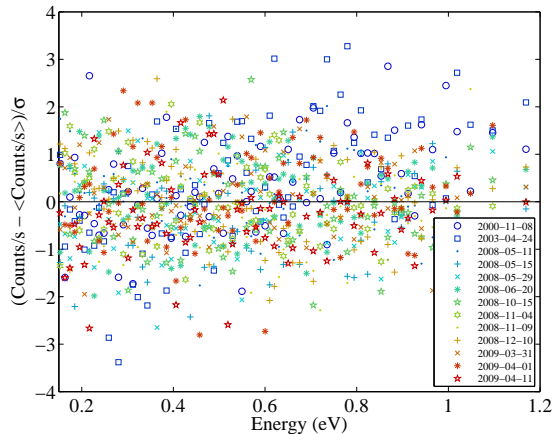


FIG. 3.— Binned EPIC-pn spectra of RX J0806, where we have subtracted off the mean spectrum and divided by the uncertainties. The background has been subtracted, but no other corrections have been done. The individual observations are labeled by their dates from Table 1.

thus infer a precise spin-down rate: the gaps are so large that even at 1σ , the uncertainty on the cycle count from the $\dot{\nu}$ uncertainty is $\frac{1}{2}\sigma_{\dot{\nu}}\Delta t^2 = 7.2$ cycles (where $\Delta t = 1.8 \times 10^8$ s is the gap between the reference time and Rev. 618).

2.2. Spectroscopic Analysis

With ~ 3 times longer total exposure time compared to H+04, we wished to see whether the basic spectral fits of H+04 are still valid and to look for possible long-term variability such as that found for RX J0720.4–3125 by de Vries et al. (2004).

To do so we examined all EPIC-pn spectra of RX J0806. (A full spectral analysis, including the EPIC-MOS and RGS data and a phase-resolved analysis, is in progress.) We used the same source and background extraction regions as for the timing analysis, created appropriate response files, and binned the spectral files such that the bin width was at least 25 eV (about one third of the spectral resolution) and the number of source plus background counts was at least 25.

We first compared the raw EPIC-pn spectra of all of the observations against each other. This did not include any response files or calibration corrections, but even so the binned pn spectra were generally consistent with each other implying no spectral change (Fig. 3). The only small deviations were seen for the archival data in 2000 and 2003 (reduced χ^2 of 2–3), and much of that could be corrected by a small slope across the 0.15–1.2 keV band: a fractional change of ≈ 0.15 keV $^{-1}$ is sufficient to get a reduced χ^2 of 1–2 for all observations. This change for the early data most likely reflects a small degree of event pileup present in those observations above 0.7 keV, caused by the 73 ms frame time of the full frame mode being insufficient to separate all events (for the small window mode, with its 6 ms frame time, pileup is not an issue). Because of this corruption, in the following fits we excluded the full frame data. We note, however, that the results including those data were still quite similar.

We fit the pn data from 2008–2009 together using *sherpa*. Like H+04, we found that an absorbed blackbody did not provide a good fit. Indeed, the deviations from a blackbody forced the interstellar absorption col-

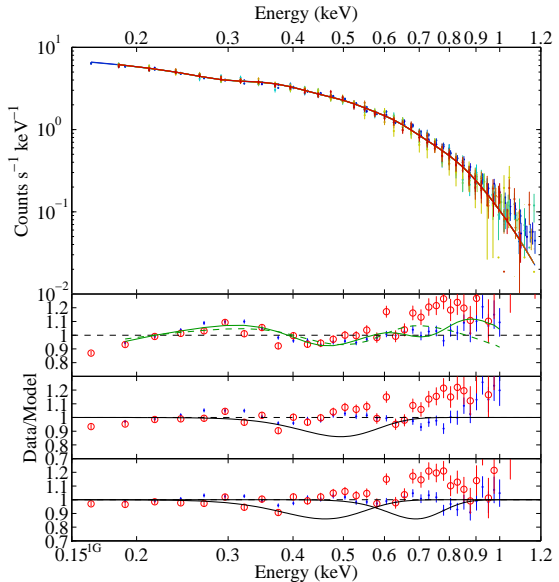


FIG. 4.— EPIC-pn spectra of RX J0806. The top panel shows the data from each observation (as in Fig. 3) along with the best-fit blackbody plus 2 absorption line model (2G; solid line). The lower panels give the ratio of the data from 2008–2009 (with all observations averaged together for clarity as the blue points, and Rev. 618 separately as the red circles) to the model for the best-fit blackbody, 1G, and 2G models (as labeled; Table 3). In the blackbody panel we plot the ratio of the models 1G/Blackbody (dashed green line) and 2G/Blackbody (solid green line). Where we have Gaussian absorption components, we also show the Gaussians schematically (black lines), although the amplitudes are on an arbitrary scale.

umn density N_{H} to zero. Rather than setting N_{H} arbitrarily, we fit for an unabsorbed blackbody: while not realistic, this provides a reference. We list the corresponding radius and temperature in Table 3. In Fig. 4, one sees that there are strong negative residuals near 0.45 keV. We tried fitting for this using Gaussian absorption lines, defined as follows,

$$F(E) = F_C(E) \left[1 - \sum_{i=1}^{N_{\text{abs}}} A_i \exp \left(-4 \ln 2 \frac{(E - E_i)^2}{\text{FWHM}_i^2} \right) \right] \quad (2)$$

where $F_C(E)$ is the continuum spectrum (a blackbody with interstellar absorption), E_i , A_i , and FWHM_i are the central energy, absorption depth, and FWHM of absorption component i and the factor of $4 \ln 2$ converts from a FWHM to a Gaussian σ .

In Fig. 4, one sees that the absorption is broad and somewhat asymmetric. We found that, as a result, if we left the FWHM free, a single Gaussian became as wide as the blackbody peak. Instead, therefore, we decided to fix the FWHM to 0.2 keV, similar to what was used by H+04 (0.16 keV). This is arbitrary, but should at least give a qualitative sense of the amount of absorption present. Including this single component results in a feature with an equivalent width of 53 eV and a significantly improved fit. As a consistency check, we kept the central energy and amplitude of the absorption fixed and fit for the FWHM, finding a best-fit value of 0.23 keV.

In Figure 4, there still appear to be significant deviations of the residuals of the 1G model near 0.65 keV, showing that our single line could not reproduce the de-

TABLE 3
RESULTS OF SPECTROSCOPIC FITS TO THE COMBINED 2008–2009 EPIC-PN DATA

Model ^a	kT^∞ ^b (eV)	R_{BB}^∞ ^b (km)	N_{H} (10^{20} cm^{-2})	E_1 ^c (eV)	A_1 ^c	E_2 ^c (eV)	A_2 ^c	F_X ^d ($10^{-12} \text{ ergs s}^{-1} \text{ cm}^{-2}$)	$F_X^{U,d}$ ($10^{-12} \text{ ergs s}^{-1} \text{ cm}^{-2}$)	χ^2/DOF
Blackbody	95.0(2)	1.432(8)	0.0	2.3	2.3	649/392
1G	95.1(11)	1.93(7)	0.95(11)	486(5)	0.25(2)	2.3	2.9	482/389
2G	87.2(11)	2.39(15)	1.7(2)	460(5)	0.42(3)	693(12)	0.26(3)	2.3	3.5	402/387

NOTE. — Only the 0.15–1.2 keV range was fitted. Quantities in parentheses are the formal $1\text{-}\sigma$ uncertainties on the last digit. Quantities without uncertainties were held fixed for that particular fit.

^a A blackbody modified by interstellar absorption, plus 0, 1, or 2 Gaussian absorption lines following Eqn. 2.

^b The effective temperature and radius of the best-fit blackbody as seen by a distant observer. The radius is scaled to a distance of 250 pc.

^c The central energy and absorption depth of Gaussian absorption lines with fixed FWHM = 200 eV. The equivalent width is $A(\pi/4 \ln 2)^{1/2} \text{FWHM} = 212.9A \text{ eV}$.

^d Absorbed and unabsorbed fluxes in the 0.2–2.0 keV band.

viations from the black body well. We therefore added a second Gaussian absorption component near that energy.⁴ This significantly improved the fit, with much flatter residuals and a reduced χ^2 of 1.04. The change in χ^2 is significant at the $\sim 10^{-16}$ level, according to an F-test. We also fit Gaussians at a range of energies across the 0.2–1.1 keV band, and find that except for the edges of the band (where the fitting breaks down) only lines near 0.68 keV give significant improvements to the fit. Compared to allowing the FWHM of the first Gaussian to vary, we find that including a second line gives a much better fit (e.g., reduced χ^2 of 1.52 for $\text{FWHM}_1 = 0.5 \text{ keV}$).

Even with two Gaussians, there is still structure in the residuals and the reduced χ^2 is not quite 1, likely reflecting the even-more complex shape of the absorption feature. The two lines in Figure 4 overlap, and there are residuals at their edges. The equivalent width of the first line has now increased to 89 eV, with the second at 55 eV. The energies of these lines are in an almost 3:2 ratio which may reflect some underlying harmonic structure to the absorption, but it may also just come from attempts to fit the complex structure of the absorption with simple shapes: changing the FWHM of each line changes the central energies and the ratio, which is almost 1.7 for lines with FWHM of 0.3 keV. We could add additional components to improve the fit but they become increasingly artificial. We did try to fit in wavelength space where the shape of the absorption is slightly different (e.g., van Kerkwijk et al. 2004). There the basic results hold, and while a single Gaussian does a somewhat better job, it is still far from perfect. Overall the absorption seems truly complex in shape, with a total equivalent width $\gtrsim 140 \text{ eV}$. Further phase-resolved fits may be able to help understand some of the complexities, but we defer them to a later paper.

While the data were largely consistent with a constant spectrum, we did one simple test in which we allowed the individual observations to differ. With the basic 2G fit from Table 3 the observations had reduced χ^2 ranging from 0.7 to 3.3, where the longest observation (Rev. 618) had the worst χ^2 . This is also evident in Figure 4, where

⁴ Haberl (2007) discussed fitting two lines in a fixed ratio, and that improved the quality of the fit (albeit with less data). However, it was not well constrained, and both of lines from Haberl (2007) would fit in the general region where we find significant residuals.

the residuals from Rev. 618 are generally similar to the average residuals, with some slight deviations at high energies. With the exceptions of the data from 2000 and 2003, we find the data are consistent with a constant spectrum. The early data deviate slightly, giving slightly higher temperature and lower radius, but again this is largely because of the pileup-induced apparent hardening of the spectrum. Even including all of the data in the fit, kT changes by only a few eV with a resulting change in the blackbody radius such that $R_{\text{BB}}^2 \propto kT_{\text{BB}}^{-4}$, i.e., the flux stayed relatively constant ($< 2\%$).

3. RX J0806.4–4123 AND THE INS

Much like the other INS for which we have derived timing solutions/constraints, RX J0806 has a magnetic field near a few by 10^{13} G (nominally, $2.5 \times 10^{13} \text{ G}$ and $< 3.7 \times 10^{13} \text{ G}$ at 2σ) with a characteristic age of a few Myr (nominally, 3.3 Myr and $> 1.5 \text{ Myr}$ at 2σ) and a spin-down luminosity of $\sim 10^{30} \text{ ergs s}^{-1}$. As such, the INS form a very homogeneous group. Here, we discuss the implications for their spectral features, as well as for the overall neutron star population.

3.1. INS spectral features

In van Kerkwijk & Kaplan (2007) we compared the X-ray absorption of the different INS to a simple model including ion cyclotron and neutral hydrogen absorption in strong magnetic fields. We noted that the absorption energy of RX J0806 ($\approx 0.45 \text{ keV}$) was similar to that of RX J1605.3+3249 (van Kerkwijk et al. 2004), and we see here that the depths are also comparable (we found 139 eV for the equivalent width of the main absorption line for RX J1605.3+3249). Haberl (2007) even found that a second line with an energy 1.5 times the first significantly improved the fit of RX J1605.3+3249, as we found here for RX J0806, making the sources even more similar, although we again caution that it is not clear how unique or meaningful those fits are. We speculated that the magnetic fields might be the same, at $\sim 10^{14} \text{ G}$ (this value is required for both proton cyclotron and neutral hydrogen transitions; also see Haberl 2007). However, even though we do not have a clear detection of spin-down and thus cannot compare in detail, we can exclude this picture for RX J0806: our limits show that at least the dipole component is quite a bit lower (see KvK09 for a similar discussion regarding RX J2143.0+0654). The possible presence of multiple lines complicates the situation

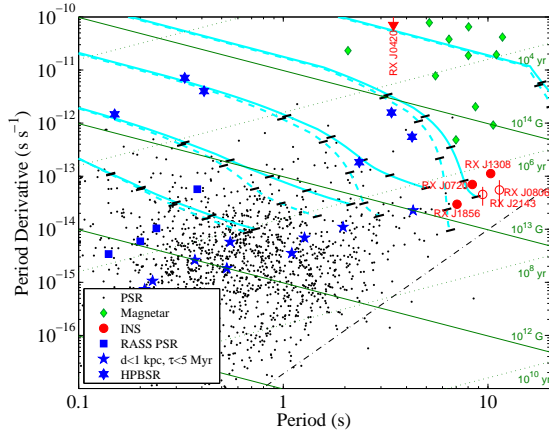


FIG. 5.— $P-\dot{P}$ diagram. We show the non-recycled pulsar population as points. The individual types of objects listed in Table 4 are also indicated: the INS are red circles (or upper limits where no \dot{P} is known), the pulsars detected by *ROSAT* are blue squares, and the nearby/young pulsars are blue five-pointed stars, and the pulsars with dipole fields $\geq 10^{13}$ G and X-ray observations are blue six-pointed stars. We also plot the magnetars (Woods & Thompson 2006) as green diamonds. We indicate lines of constant dipolar field and characteristic age as labeled. Finally, we also show the results of evolutionary model from Pons et al. (2009) as the thick lines (solid lines: dipole only; dashed lines: including a toroidal component with a strength of 50 times that of the dipole). The initial dipole fields are $10^{13,13.5,14,14.5,15}$ G at the pole, there are cross-ticks at (0.01, 0.03, 0.1, 0.3, 1) Myr, we assumed initial periods of 0.1 s, and we have divided the field at the pole by 2 to get the field at the equator for comparison with the spin-down field estimates (see Lorimer & Kramer 2004).

somewhat, since the “fundamental” may be at lower energies and thus the inferred magnetic field weaker. However, since harmonics should be significantly weaker for ion cyclotron resonance at least (Pavlov & Panov 1976), this seems unlikely to be the explanation.

Presuming that the absorption comes from some transition in the atmosphere, there are a number of alternative explanations. For one, the magnetic field geometry could play a role. The dipole component that we measure is only a projection of the true dipole field, and the field on the surface could have higher order or substantial toroidal components (Braithwaite 2009). Beyond that, different INS could have different chemical composition, although then we have to understand how the apparent emission radii of the INS are relatively similar (Kaplan et al. 2007).

Including RX J0806 in the magnetic field-effective temperature plane, it is consistent with the line defined by RX J1856.5–3754 RX J0720.4–3125, and RX J1308.6+2127 (KvK09). As discussed in KvK09, this correlation, while quite possibly a coincidence, may have some relation to the origin of the INS and the coupling of the magnetic and thermal evolutions (see below). It is also possible that it is influenced by surface condensation⁵ (Medin & Lai 2007).

3.2. The INS, and the Neutron Star Population

While the INS were discovered over 10 years ago, we still lack a detailed appreciation for their place in the

⁵ In our discussion of the effects of condensation in KvK09, we incorrectly stated that a condensed surface would inhibit a vacuum gap and hence radio emission: in fact it is the opposite (Z. Medin 2009, priv. comm.).

overall neutron star population and for what makes them unique (although see Popov et al. 2000b,a, 2006, 2008 and references therein for some discussion). A full understanding requires detailed models of the birth and evolution of neutron stars, but given the small numbers of objects and the large number of free parameters, getting reliable constraints is necessarily difficult. However, we can gain some insight by comparing the INS to different related neutron star populations. For this purpose, we give the salient properties of different objects in Table 4. Aside from the seven confirmed INS, we consider:

- Rotation-powered pulsars detected in the *ROSAT* All-sky Survey with count-rates $\geq 0.05 \text{ s}^{-1}$ in the PSPC (referred to here as “RASSPSRs”).
- Other relatively young and nearby rotation-powered pulsars (referred to here as “NearPSRs”; we adopted a distance limit of 1 kpc and a characteristic age limit of 5 Myr).
- Rotation-powered pulsars with dipole magnetic field $\geq 10^{13}$ G (so called high- B pulsars, or “HPBSRs”), but limited to those with X-ray observations.

These objects each make appropriate comparisons with the INS. The RASSPSRs are generally young and nearby neutron stars (we exclude the Crab pulsar from further consideration as it is much younger and more distant than the rest of the RASSPSRs), with X-ray luminosities and distances similar to those of the INS. Moreover, these were all detected in the same survey that discovered the INS. However, we do not know exactly how young the INS are. We therefore also include the NearPSRs: a sample of moderately young, moderately nearby pulsars regardless of their X-ray luminosity. While the INS are likely within 500 or 700 pc, we extend our range to 1 kpc for the pulsars since the distances of both classes are uncertain. Similarly, we extend to characteristic ages of 5 Myr, compared to characteristic ages of ~ 3 Myr for the INS and kinematic ages of < 1 Myr. Finally, as the INS have larger than average magnetic fields, we also include those HPBSRs that have comparable dipole fields ($\geq 10^{13}$ G) and X-ray observations.

For each object, we give:

- The timing properties, comprising the spin-period and the properties derived from that and \dot{P} : dipole magnetic field, characteristic age, and spin-down luminosity. With the exception of RX J2143.0+0654 and RX J0806 (where the spin-down measurements are only marginally significant) these data are uniformly of high quality.
- The X-ray spectral properties, comprising the count-rate (as detected in the *ROSAT* PSPC), temperature and radius of the best-fit blackbody, luminosity of the blackbody, and total luminosity including any non-thermal components. The quality of these parameters varies by object. For the INS they are relatively uniform, but the details of the spectral fit depend on the observations and the object as different objects have different levels of X-ray absorption (for example see

van Kerkwijk & Kaplan 2007, §§ 2.2 and 3.1). For the RASSPSRs the thermal components are from just one possible decomposition, and often two blackbodies are required in addition to a non-thermal component. For the fainter NearPSRs and HBPSRs again there are problems of decomposition (now limited by signal-to-noise ratio), and in many cases we only have upper limits.

- The distance (measured by astrometry where available) and any other age indicator (kinematic age or age of associated supernova remnant). Distances from astrometry are ideal, but in marginally-significant cases (such as RX J0720.4–3125; Kaplan et al. 2007) Lutz-Kelker bias (Lutz & Kelker 1973; Smith 2003) can make them appear closer than they are, although other information such as X-ray absorption and Galactic geometry can be incorporated to improve the situation. For objects without astrometry, we rely on the dispersion measure (in radio) and hydrogen column densities (in X-rays) along with models for the Galaxy. In both cases, the results can be unreliable, especially for close objects (as these are), although it is less likely that they are systematically biased. Furthermore, the X-ray absorption column density can be unreliable as it is often covariant with other fitting parameters as well as with the assumed shape of the spectrum (e.g., Durant & van Kerkwijk 2006).

For additional notes on the data, see Table 4.

If we take the RASSPSRs and INS as a single sample detected by *ROSAT*, the two groups have roughly comparable sizes (Popov et al. 2003; Kaplan 2004, 2008). Based on their temperatures and independent ages at least some of the RASSPSRs may be slightly younger than the INS, but the temperatures can be affected by non-thermal emission processes absent in the INS. Comparing the INS to the RASSPSRs, the INS have comparable X-ray luminosities of $\sim 10^{32}$ erg s $^{-1}$ (e.g., Popov et al. 2003; Kaplan 2004, 2008). The kinematic ages of the INS (when available) are comparable to if not slightly larger than the ages of the RASSPSRs. However, the characteristic ages of the RASSPSRs are also small, < 1 Myr, while the characteristic ages of the INS are all > 2 Myr. All of the RASSPSRs have periods < 0.4 s, while the INS have periods an order of magnitude longer and considerably stronger magnetic fields.⁶ In contrast, for the slightly older NearPSRs the characteristic ages are often comparable to those of the INS but the X-ray luminosities are several orders of magnitude lower ($\sim 10^{29}$ erg s $^{-1}$). The INS also have much lower \dot{E} than any other population. Finally, we note that INS have larger radii and smaller effective temperatures for the same X-ray luminosity. Is this an innate difference, perhaps as a result of the magnetic field geometry? Or is it artificial, perhaps a consequence of unrealistic emission models?

⁶ At some level, our comparison of magnetic fields, pulse periods, characteristic ages, and spin-down luminosities is degenerate since these parameters are all related. Nonetheless, we will continue to emphasize differences among multiple parameters when appropriate.

As we discussed previously (e.g., KvK05a), we need to reconcile the discrepant kinematic and characteristic ages of the INS. For one or two objects it could be a coincidence, but even for the objects without kinematic ages (RX J0806, RX J2143.0+0654), the luminosities suggest the true ages are substantially shorter than the characteristic ages. While having a very long initial period is possible, it would have to be very close to the current value. For other sources where the characteristic ages exceed the true ages, like PSR J0538+2817 (Kramer et al. 2003a; Ng et al. 2007), the initial spin period required in order to have spun-down to their current periods in their true ages (assuming dipole braking) is < 0.2 . This is longer than the traditionally-assumed ~ 30 ms (Lyne, Pritchard, & Graham-Smith 1993; Migliazzo et al. 2002), but similar to the more recently favored periods of a few hundred ms (Kramer et al. 2003a; Vranesevic et al. 2004; Gotthelf, Halpern, & Seward 2005; Faucher-Giguère & Kaspi 2006), and, most relevant for the present purposes, much smaller than what would be required for the INS ($\gtrsim 5$ s).

Kramer et al. (2006) have discovered a pulsar whose spin-down torque varies quasi-periodically along with its radio emission. For approximately 10–20% of the time PSR B1931+24 (an otherwise ordinary pulsar with characteristic age of 1.6 Myr and dipole field of 2.6×10^{12} G) is visible as a radio pulsar, but for the remaining time the radio emission is not detectable and the torque is reduced to $\frac{2}{3}$ of its normal value. The difference is attributed to the presence (or strength) of an energetic plasma wind, where a strong wind leads to radio emission and higher torque. While we suspect from its H α nebula that RX J1856.5–3754 does indeed have an energetic wind and brakes by magnetic dipole radiation, that scenario is not completely self-consistent (see below). So the absence of radio emission from the INS may point to cessation (or at least diminution) of a wind and its associated torque, and this could be a recent development in the histories of the sources if radio emission has just shut off. If the wind/radio emission only stopped recently (the worst case scenario) then the period evolution would have been dominated by a spin-down approximately $\frac{3}{2}$ times what we see now and the characteristic age that we measure now would be high by 50%. This would go some but not all of the way toward resolving the discrepancy between the timing and kinematic ages, although differences in geometry (also see KvK09) could lead to slightly larger factors (other intermittent pulsars have since been discovered with slightly larger ratios of 1.7 instead of 1.5, possibly due to differences in alignment between the rotation and magnetic axes; Kramer 2008). Such a comparison also suggests that there could be torque and/or radio flux variations in the INS, neither of which has been seen (except for the one timing/spectral change for RX J0720.4–3125; van Kerkwijk et al. 2007) but the sampling has been very sparse.

Another possibility is that spin-down does not follow the expectations for magnetic dipole radiation. For instance, a decaying magnetic field would give rise to a situation like what we see for the INS, as it would allow the sources to spin down rapidly early in their evolution (KvK09). Field decay was proposed previ-

ously for the INS as a way to keep them hotter longer and thereby make them overrepresented in a local sample (Heyl & Kulkarni 1998). Initial timing results suggested that field decay was not presently heating the INS (Zane et al. 2002; Kaplan et al. 2002b), and indeed the INS have roughly the expected thermal luminosities for their kinematic ages (especially given the large uncertainties and the steep decline in thermal luminosity for objects of this age; see e.g., Page et al. 2004). However, as we discuss below, field decay may have profoundly affected the magnetic and rotational evolution of the INS, and may have some other visible consequences. The models of field decay used by Kaplan et al. (2002b) were rudimentary, and including decay by other modes as well as a strong toroidal component can greatly change the outcome.

Regardless of the specific model, if the characteristic ages are correct for the INS, they are too luminous by more than a factor of 100 to be powered by residual heat. They would therefore require an extra energy source which we know cannot be the spin-down luminosity: the remaining alternative is magnetic field decay. If instead (and as we believe) the kinematic ages are correct, then the X-ray luminosities are reasonable, but we need to explain the long periods (and the associated large characteristic ages, low spin-down luminosities). Again, magnetic field decay seems to be the best option.

3.3. *The INS and a Model of Magnetic Field Decay*

The coupled magnetic and thermal evolution for neutron stars was studied in detail by Pons et al. (2009). These authors assumed a range of initial field and temperature configurations and then followed them over time. Briefly, they found that for all sources with initial magnetic fields $\gtrsim 5 \times 10^{13}$ G, the final magnetic field is $\sim 3 \times 10^{13}$ G at 0.5 Myr. But for all sources with weaker initial magnetic field the final magnetic field is just half the initial field. We note that the model of Pons et al. (2009) assumes magnetic field configurations and mechanisms of decay that may well be overly simplified. One of the biggest free parameters in their models is the ratio of toroidal to poloidal fields. This can vary significantly (e.g., Braithwaite 2009), and the non-linearity of field decay means that a strong, decaying toroidal component can alter the weaker poloidal component while being otherwise invisible.

Despite the above uncertainties, it seems encouraging that the main findings of Pons et al. (2009) for the results of field decay are similar to what we infer for the INS: neutron stars grouped around 2×10^{13} G at true ages of ~ 0.5 Myr or older. Taking the magnetic field evolution and using it to infer the spin-down history, one expects that neutron stars with strong fields quickly move across the $P - \dot{P}$ diagram, losing memory of the initial spin period. We find that as long as the initial field is between 1×10^{14} G and 7×10^{14} G, then the neutron star ends up at a period of 3 to 15 s (Fig. 5). Coupling the thermal evolution in with the magnetic field, Pons et al. (2009) find luminosities of $\sim 10^{32}$ erg s $^{-1}$ at ages of ~ 0.5 Myr, similar to what is expected for less strongly magnetized neutron stars; the excess energy from the field decay is mostly radiated at earlier ages, with the thermal luminosity being substantially higher around 10^5 yr. At ~ 0.5 Myr,

the difference may still be a factor of a few (dependent on field configuration and strength), but this would be largely lost in the observational uncertainties (age, distance, etc.). This small remaining difference should not lead to a great over-representation in a local sample, and therefore the fact that about half of the young neutron stars detected by *ROSAT* (the INS plus the RASSPSRs) have long periods (and presumably strong fields) should give a reasonable clue to the true population. In a bit more detail, this will depend on the slope of the cooling curve: for power-law cooling $L \propto t^{-\alpha}$, increasing the luminosity by a factor of λ will lead to an increase in population size of $\lambda^{-1/\alpha}$ in a flux-limited sample if the population is in a constant volume (as might be expected for soft X-ray sources, since the exponential cutoff of interstellar absorption limits their detectability to $\lesssim 1$ kpc). If the volume can increase too, we get an additional factor of λ in the population (assuming the population is confined to the Galactic disk). The true situation will probably be in between these extremes. With α typically between 2 and 3 at a few 10^5 yr (for photon cooling), a factor of at most a few increase in luminosity (due to field decay) would lead to a factor of $\lesssim 2$ increase in population. Therefore, the INS would represent between one quarter and half the total population.

As an aside, we note that an interesting implication of the model of Pons et al. (2009) is that neutron stars may be hotter on the equator than at the poles, a combination of Joule heating from field decay and reduced conductivity preventing the heat from going inward. While the effect may be quite small at the ages of the INS, this may still complicate the interpretation of the lightcurve and phase-resolved spectroscopy of the INS. Typically, a model with a warm pole and cool equator is assumed (e.g., Braje & Romani 2002; Ho 2007), although more complicated models have also been considered (Zane & Turolla 2006). If the geometry were reversed that could lead to different interpretations, and work is on-going to see if there are clear consequences to that (W. C. G. Ho, 2009, pers. comm.). The asymmetry between equator and pole is time- and field-dependent, being most apparent for strong fields and at early times. For weak fields, the standard hot poles are regained. It may be that the very low pulsed fractions and limits found in sources like RX J1856.5–3754 and RX J1605.3+3249 are a consequence of being near the time where the surface becomes nearly isothermal, and that this underlies the difficulty in finding geometries that satisfy the observed pulsation limits (Braje & Romani 2002; Ho 2007). If there is still a strong, buried toroidal field it could also lead to some ongoing, low-level decay, which might give rise to some of the spectral and temporal evolution seen in RX J0720.4–3125 (de Vries et al. 2004; Vink et al. 2004; Haberl et al. 2006; van Kerkwijk et al. 2007), although nothing similar has been seen in the long-term monitoring of other sources (§ 3.1; Haberl 2007; KvK09).

If, as we posit, magnetic field decay has influenced the period evolution of the INS, we can ask what the progenitors and descendants of the INS might be. Heyl & Kulkarni (1998) discussed RX J0720.4–3125 as an old magnetar. This could still be the case, although based on the models of Pons et al. (2009) the initial mag-

netic fields for the INS would be close to $\sim 3 \times 10^{14}$ G and not much higher and would have followed an evolution that only skimmed the parameter range occupied by the magnetars (see Fig. 5). The descendants of the stronger-field magnetars would be expected to end up with longer periods. The INS do not actually seem to be old versions of at least the X-ray-bright HBPSRs. These HBPSRs mostly have $\dot{E} > 10^{36}$ erg s $^{-1}$ (although this may partly be a selection effect, as this would increase L_X). Using the model of Pons et al. (2009) and evolving typical HBPSRs to ages of 0.5 Myr, we would expect $\dot{E} \sim 10^{32}$ erg s $^{-1}$, which exceeds by an order of magnitude what the INS have. These HBPSRs may in fact have magnetic fields close to their initial values with little decay, while the INS started with $\gtrsim 10^{14}$ G and have decayed. A few of the HBPSRs, like PSR B0154+61 ($\log_{10} \dot{E} = 32.8$, $\log_{10} L_X < 32.3$), PSR J1819–1458 ($\log_{10} \dot{E} = 32.5$, $\log_{10} L_X = 33.7$), and PSR J1718–3718 ($\log_{10} \dot{E} = 33.3$, $\log_{10} L_X \approx 33.5$), may be more similar, although we have no independent age estimates for those objects. Of these, the comparison to PSR J1819–1458 may be particularly interesting, as it emits only sporadic radio bursts as a so-called “Rotating Radio Transient” (RRAT; McLaughlin et al. 2006). The possibilities of a connection between the RRATs and the INS have already been discussed in several places (e.g., Popov et al. 2006), but the spectral similarities (McLaughlin et al. 2007) and the recent detection of extended X-ray emission from PSR J1819–1458 that seems too large for its \dot{E} (Rea et al. 2009) highlight it even further. The connection can only go so far, though: searches for RRAT-like radio emission from the INS have not been successful (Kondratiev et al. 2009).

As for the descendants of the INS, while they might be too faint for X-ray detection, they could still be apparent in radio surveys (although there are observational selection effects against long-period objects). However, very few objects are known in that part of the $P - \dot{P}$ diagram, and there are not enough to span the expected ages of up to 10^7 yr. Does this mean that the old INS have very narrow radio beams that miss the Earth, therefore reducing their prevalence in radio surveys? Or are there no radio beams? Will the surfaces condense to allow the formation of vacuum gaps (Medin & Lai 2007) or is this inhibited? This is largely a function of composition and state, which, as we discussed, remains uncertain. The H α nebula around RX J1856.5–3754 might be taken as evidence for the generation of energetic particles (van Kerkwijk & Kulkarni 2001; Kaplan et al. 2002c), but the required \dot{E} is far higher than what is inferred from timing (van Kerkwijk & Kaplan 2008).

One interesting object that may bridge the gap between the standard pulsars and the INS is PSR B1845–19: its long period and characteristic age put it within reach of the INS, although we do not have an independent age or X-ray luminosity. Compared to the INS, the \dot{E} for this object is slightly higher, while the characteristic age is similar, possibly suggesting that it sits at the boundary where magnetic field decay becomes important ($\gtrsim 10^{13}$ G, according to Pons et al. 2009). Just how close the actual age is to the characteristic age may prove an important test of this scenario.

4. CONCLUSIONS

We have presented initial results from coherent timing of the nearby neutron star RX J0806. While we were not able to obtain a statistically significant measurement of spin-down, we were able to constrain the spin-down rate (and hence the dipolar magnetic field) to rather low values, and with the addition of a few data points with longer time baselines we should achieve a reliable measurement. The limit on the magnetic field ($< 3.7 \times 10^{13}$ G at 2σ) is interesting, as it is considerably lower than the $\sim 10^{14}$ G expected from simple models of the X-ray spectrum. This echoes the discrepancy seen in RX J2143.0+0654 (KvK09), suggesting that we need to develop an improved model for the X-ray spectra of the INS. Whether this is just from an improved treatment of the radiative transitions (e.g., auto-ionizing transitions may play a role) or elements beyond hydrogen we do not know, but ongoing work in obtaining better timing constraints as well as phase-resolved spectroscopy should help to narrow the possibilities.

The X-ray spectrum of RX J0806 shows clear signs of a broad absorption feature at 0.3–0.6 keV, and our data show that it cannot be simply modeled by one or even two Gaussians. The pulsations are also relatively strong in the same spectral region, giving some hope that phase-resolved spectroscopy will allow us to illuminate the possible decompositions.

Comparing the INS with other relevant sub-populations of neutron stars, we are led to the conclusion that magnetic field decay has operated over the ~ 0.5 Myr lifetimes of the INS. This can be seen from a qualitative comparison of the observed X-ray luminosities of the INS with X-ray luminosities of other sources and with predictions from standard cooling curves. From both, one infers that the characteristic ages are systematically long, while the kinematic ages are consistent with cooling models and the ages of other neutron stars with comparable luminosities. This conclusion is supported by the detailed modeling of Pons et al. (2009), whose expectations for neutron stars born with magnetic fields of $\sim 2 \times 10^{14}$ G evolved to ~ 0.5 Myr greatly resemble the INS. Among the implications of this model are that some neutron stars with magnetic field decay should be hotter at the equator than at the poles, in contrast with most assumed models of neutron star surface temperature distributions. Once again, phase-resolved spectroscopy would seem to be one of the best ways to try to discriminate between the possibilities. Improved models for the surface temperature, which constrain the viewing geometry, can then also be combined with proper motion measurements to try to understand some aspects of the complicated relation between magnetic fields, rotation, and kick velocities in young neutron stars (Lai 2001).

We thank A. Spitkovsky for helpful discussions. Based on observations obtained with XMM-Newton, an ESA science mission with instruments and contributions directly funded by ESA Member States and NASA. DLK was supported by NASA through Hubble Fellowship grant #01207.01-A awarded by the Space Telescope Science Institute, which is operated by the Association of Universities for Research in Astronomy, Inc., for NASA, under contract NAS 5-26555. This research was sup-

TABLE 4
PROPERTIES OF THE ISOLATED NEUTRON STARS AND RELATED ROTATION-POWERED PULSARS

Source	Timing ^a				Spectrum ^b					d ^c (pc)	Age ^d (Myr)	Refs.
	P (s)	B_{dip} (10^{12} G)	τ_{char} (Myr)	$\log_{10} \dot{E}$ (erg s^{-1})	PSPC (s^{-1})	kT (eV)	R_{BB} (km)	$\log_{10} L_{X,\text{BB}}$ (erg s^{-1})	$\log_{10} L_{X,\text{tot}}$ (erg s^{-1})			
Isolated Neutron Stars												
RX J1308.6+2127	10.31	34	1.5	30.6	0.3	102	4.1	32.4	32.4	500	0.8–1.2	1; 2; 3; 4; 5; 6
RX J0720.4–3125	8.39	24	1.9	30.7	1.6	87	6.4	32.5	32.5	360	0.5–1.0	7; 8; 9; 10; 11; 12
RX J0806.4–4123 ^e	11.37	25	3.3	30.2	0.4	92	1.3	31.2	31.2	250	...	13; 14, this work
RX J2143.0+0654	9.44	20	3.7	30.3	0.2	102	3.2	32.1	32.1	430	...	15; 16; 17; 18; 19
RX J1856.5–3754	7.06	15	3.8	30.5	3.6	62	6.2	31.9	31.9	160	0.4	20; 21; 22
RX J1605.3+3249	0.9	93	4.7	32.3	32.3	390	0.1–1.0	23; 24; 14; 25; 26
RX J0420.0–5022	3.45	0.1	45	3.3	30.8	30.8	345	...	13; 14
Rotation Powered Pulsars with PSPC $> 0.05 \text{ s}^{-1}$ (RASSPSRs)												
Crab	0.03	3.8	0.0012	38.7	48.4	37.6	2000	0.001	27
Vela	0.09	3.4	0.011	36.8	3.4	128	2.1	32.3	32.8	287	0.01	28; 29
PSR B0656+14	0.38	4.7	0.11	34.6	1.92	56	20.9	32.7	32.7	288	0.1	30; 31; 32
PSR B1951+32	0.04	4.9	0.11	36.6	0.07	130	2.1	32.2	33.3	2000	0.06	33; 34
Geminga	0.24	1.6	0.3	34.5	0.54	43	8.6	31.9	31.8	250	...	32; 35
PSR B1055–52	0.20	1.1	0.5	34.5	0.35	68	12.3	32.6	32.6	750	...	36; 32
PSR J0538+2817	0.14	0.7	0.6	34.7	0.06	160	3.2	32.9	32.9	1470	0.04	37; 38
Rotation Powered Pulsars with $d < 1 \text{ kpc}$, $\tau_{\text{char}} < 5 \text{ Myr}$ (NearPSRs)												
PSR J1741–2054	0.41	2.7	0.4	34.0	31.1	400	...	39
PSR B0450–18	0.55	1.8	1.5	33.1	760	...	40
PSR B0450+55	0.34	0.9	2.3	33.4	1190	...	40
PSR J1918+1541	0.37	1.0	2.3	33.3	680
PSR B0628–28	1.24	3.0	2.8	32.2	0.003	< 29.4	30.1	332	...	41; 42
PSR B2045–16	1.96	4.7	2.8	31.8	950	2	40
PSR B1845–19	4.31	10.1	2.9	31.1	950
PSR B0834+06 ^f	1.27	3.0	3.0	32.1	...	170	0.03	29.0	29.0	640	...	43
PSR B1929+10	0.23	0.5	3.1	33.6	0.012	300	0.03	30.0	30.4	361	1–2	44; 45
PSR J1908+0734	0.21	0.4	4.1	33.5	< 0.005	790	...	46
PSR B0823+26	0.53	1.0	4.9	32.7	0.0016	< 101	0.2 ^g	< 29.7	29.4	360	...	47
PSR B0943+10 ^h	1.10	2.0	5.0	32.0	...	270	0.02	28.7	28.7	630	...	48
Pulsars With $B \geq 10^{13} \text{ G}$ and X-ray Observations (HBPSRs)												
PSR J1119–6127	0.41	41	0.0016	36.3	...	210	3.2	33.4	33.6	8400	< 0.01	49; 50; 51; 52
PSR B1509–58	0.15	15	0.0016	37.3	34.3	5200	0.006–0.02	53; 54; 55
PSR J1846–0258 ⁱ	0.33	49	0.0007	36.9	34.5	6000	< 0.001	56; 57; 58
PSR J1124–5916	0.14	10	0.002	37.0	...	< 102	12 ^j	< 33.3	33.1	6000	0.03	59; 60
PSR J1930+1852	0.14	10	0.002	37.0	34.6	6200	...	61; 62; 63
PSR J1718–3718	3.38	74	0.03	33.3	...	145	7.7	33.5	33.5	4500	...	64
PSR J1819–1458	4.26	50	0.12	32.5	...	140	11	33.7	33.7	3600	...	65
PSR B0154+61	2.35	21	0.2	32.8	...	< 63	10 ^j	< 32.3	< 32.3	1700	...	66

REFERENCES. — 1: Kaplan, Kulkarni, & van Kerkwijk (2002a); 2: Kaplan & van Kerkwijk (2005b); 3: Haberl et al. (2003); 4: Schwope et al. (2005); 5: Schwope et al. (2007); 6: Motch et al. (2009); 7: Kaplan et al. (2003b); 8: Motch et al. (2003); 9: Kaplan & van Kerkwijk (2005a); 10: Kaplan et al. (2007); 11: van Kerkwijk et al. (2007); 12: Haberl et al. (2004a); 13: Haberl et al. (2004b); 14: Haberl (2007); 15: Zampieri et al. (2001); 16: Zane et al. (2005); 17: Rea et al. (2007); 18: Zane et al. (2008); 19: Kaplan & van Kerkwijk (2009); 20: Burwitz et al. (2003); 21: van Kerkwijk & Kaplan (2007); 22: van Kerkwijk & Kaplan (2008); 23: Kaplan, Kulkarni, & van Kerkwijk (2003a); 24: van Kerkwijk et al. (2004); 25: Motch et al. (2005); 26: Zane et al. (2006); 27: Willingale et al. (2001); 28: Pavlov et al. (2001); 29: Dodson et al. (2003); 30: Marshall & Schulz (2002); 31: Brisken et al. (2003); 32: De Luca et al. (2005); 33: Migliazzo et al. (2002); 34: Li, Lu, & Li (2005); 35: Faherty, Walter, & Anderson (2007); 36: Kramer et al. (2003b); 37: Romani & Ng (2003); 38: Ng et al. (2007); 40: Chatterjee et al. (2009); 43: Gil et al. (2008); 44: Chatterjee et al. (2004); 45: Misanovic, Pavlov, & Garmire (2008); 46: Becker & Trümper (1997); 47: Becker et al. (2004); 48: Zhang, Sanwal, & Pavlov (2005); 49: Crawford et al. (2001); 50: Caswell et al. (2004); 51: Gonzalez et al. (2005); 52: Safi-Harb & Kumar (2008); 53: Greiveldinger et al. (1995); 54: Gaensler et al. (1999); 55: Gaensler et al. (2002); 56: Leahy & Tian (2008); 57: Gavriil et al. (2008); 58: Kumar & Safi-Harb (2008); 59: Gaensler & Wallace (2003); 60: Hughes et al. (2003); 61: Lu et al. (2002); 62: Camilo et al. (2002); 63: Leahy, Tian, & Wang (2008); 64: Kaspi & McLaughlin (2005); 65: McLaughlin et al. (2007); 66: Gonzalez et al. (2004);

NOTE. — General pulsar data were taken from Possenti et al. (2002), Kaplan et al. (2004), and Manchester et al. (2005). Within each class the objects are ordered by increasing characteristic age.

^a Spin period P , dipole magnetic field $B_{\text{dip}} = 3.2 \times 10^{19} \sqrt{P\dot{P}}$, characteristic age $\tau_{\text{char}} = P/2\dot{P}$, and spin-down energy loss rate $\dot{E} = 3.9 \times 10^{46} \dot{P}/P^3$.

^b *ROSAT* PSPC count rate (if known), effective temperature and radius (for spherical emission) of the best-fit blackbody component as measured at infinity, bolometric blackbody luminosity, and total luminosity in the 0.1–2.4 keV band. For sources with multiple blackbody components, we took the one with larger radius/smaller temperature.

^c Parallax distance if known. If not, for the INS we use distances based on X-ray absorption (Posselt et al. 2007) or 500 pc for RX J1308.6+2127, while for pulsars we use distances from dispersion measures (Cordes & Lazio 2002).

^d Independent age estimate. For the INS, this is the kinematic age, derived from tracing the object back to a probable birth site. The range is based on the observed range in distance as well as the result of multiple possible birth sites. For pulsars this is either a kinematic age or an age estimate for the associated supernova remnant.

^e Here we use the nominal values for the spin-down from Table 2: using the upper limits does not change the conclusions.

^f The X-ray data are consistent with no non-thermal emission, but such emission cannot be ruled out.

^g The radius was assumed to be that of a polar cap.

^h The emission from this source is also consistent with non-thermal emission with luminosity $\sim 2 \times 10^{29} \text{ erg s}^{-1}$.

ⁱ The X-ray source is variable, and was observed at a level of about $10\times$ the previous flux (Gavriil et al. 2008; Kumar & Safi-Harb 2008).

^j The radius was fixed to that of the whole surface.

ported in part by the National Science Foundation under Grant No. PHY05-51164. MHvK acknowledges funding from NSERC. Apart from the XMMSAS data reduction pipelines provided by *XMM-Newton*, this research

has made use of software provided by the Chandra X-ray Center (CXC) in the application packages CIAO and Sherpa.

Facilities: XMM (EPIC)

REFERENCES

- Becker, W., Jessner, A., Kramer, M., Testa, V., & Howaldt, C. 2005, *ApJ*, 633, 367
- Becker, W. & Trümper, J. 1997, *A&A*, 326, 682
- Becker, W., Weisskopf, M. C., Tennant, A. F., Jessner, A., Dyks, J., Harding, A. K., & Zhang, S. N. 2004, *ApJ*, 615, 908
- Braithwaite, J. 2009, *MNRAS*, 397, 763
- Braje, T. M. & Romani, R. W. 2002, *ApJ*, 580, 1043
- Brisken, W. F., Thorsett, S. E., Golden, A., & Goss, W. M. 2003, *ApJ*, 593, L89
- Burwitz, V., Haberl, F., Neuhäuser, R., Predehl, P., Trümper, J., & Zavlin, V. E. 2003, *A&A*, 399, 1109
- Camilo, F., Lorimer, D. R., Bhat, N. D. R., Gotthelf, E. V., Halpern, J. P., Wang, Q. D., Lu, F. J., & Mirabal, N. 2002, *ApJ*, 574, L71
- Camilo, F. et al. 2009, *ApJ*, in press, arXiv:0908.2626
- Cash, W. 1979, *ApJ*, 228, 939
- Caswell, J. L., McClure-Griffiths, N. M., & Cheung, M. C. M. 2004, *MNRAS*, 352, 1405
- Chatterjee, S., et al. 2009, *ApJ*, submitted
- Chatterjee, S., Cordes, J. M., Vlemmings, W. H. T., Arzoumanian, Z., Goss, W. M., & Lazio, T. J. W. 2004, *ApJ*, 604, 339
- Cordes, J. M. & Lazio, T. J. W. 2002, astro-ph/0207156
- Crawford, F., Gaensler, B. M., Kaspi, V. M., Manchester, R. N., Camilo, F., Lyne, A. G., & Pivovarov, M. J. 2001, *ApJ*, 554, 152
- De Luca, A., Caraveo, P. A., Mereghetti, S., Negroni, M., & Bignami, G. F. 2005, *ApJ*, 623, 1051
- de Vries, C. P., Vink, J., Méndez, M., & Verbunt, F. 2004, *A&A*, 415, L31
- Deller, A. T., Tingay, S. J., Bailes, M., & Reynolds, J. E. 2009, *ApJ*, 701, 1243
- Dodson, R., Legge, D., Reynolds, J. E., & McCulloch, P. M. 2003, *ApJ*, 596, 1137
- Durant, M. & van Kerkwijk, M. H. 2006, *ApJ*, 650, 1082
- Faherty, J., Walter, F. M., & Anderson, J. 2007, *Ap&SS*, 308, 225
- Faucher-Giguère, C.-A. & Kaspi, V. M. 2006, *ApJ*, 643, 332
- Gaensler, B. M., Arons, J., Kaspi, V. M., Pivovarov, M. J., Kawai, N., & Tamura, K. 2002, *ApJ*, 569, 878
- Gaensler, B. M., Brazier, K. T. S., Manchester, R. N., Johnston, S., & Green, A. J. 1999, *MNRAS*, 305, 724
- Gaensler, B. M. & Wallace, B. J. 2003, *ApJ*, 594, 326
- Gavriil, F. P., Gonzalez, M. E., Gotthelf, E. V., Kaspi, V. M., Livingstone, M. A., & Woods, P. M. 2008, *Science*, 319, 1802
- Gil, J., Haberl, F., Melikidze, G., Geppert, U., Zhang, B., & Melikidze, Jr., G. 2008, *ApJ*, 686, 497
- Gonzalez, M. E., Kaspi, V. M., Camilo, F., Gaensler, B. M., & Pivovarov, M. J. 2005, *ApJ*, 630, 489
- Gonzalez, M. E., Kaspi, V. M., Lyne, A. G., & Pivovarov, M. J. 2004, *ApJ*, 610, L37
- Gotthelf, E. V., Halpern, J. P., & Seward, F. D. 2005, *ApJ*, 627, 390
- Greiveldinger, C., Caucino, S., Massaglia, S., Oegelman, H., & Trussoni, E. 1995, *ApJ*, 454, 855
- Haberl, F. 2007, *Ap&SS*, 308, 181
- Haberl, F., Motch, C., & Pietsch, W. 1998, *Astronomische Nachrichten*, 319, 97
- Haberl, F., Schwope, A. D., Hambaryan, V., Hasinger, G., & Motch, C. 2003, *A&A*, 403, L19
- Haberl, F., Turolla, R., de Vries, C. P., Zane, S., Vink, J., Méndez, M., & Verbunt, F. 2006, *A&A*, 451, L17
- Haberl, F. & Zavlin, V. E. 2002, *A&A*, 391, 571
- Haberl, F., Zavlin, V. E., Trümper, J., & Burwitz, V. 2004a, *A&A*, 419, 1077
- Haberl, F. et al. 2004b, *A&A*, 424, 635
- Heyl, J. S. & Kulkarni, S. R. 1998, *ApJ*, 506, L61
- Ho, W. C. G. 2007, *MNRAS*, 380, 71
- Ho, W. C. G., Kaplan, D. L., Chang, P., van Adelsberg, M., & Potekhin, A. Y. 2007, *MNRAS*, 375, 821
- Hughes, J. P., Slane, P. O., Park, S., Roming, P. W. A., & Burrows, D. N. 2003, *ApJ*, 591, L139
- Jansen, F., et al. 2001, *A&A*, 365, L1
- Kaplan, D. L. 2004, Ph.D. Thesis, California Institute of Technology
- 2008, AIPC, 983, 331, arXiv:0801.1143
- Kaplan, D. L., Frail, D. A., Gaensler, B. M., Gotthelf, E. V., Kulkarni, S. R., Slane, P. O., & Nechita, A. 2004, *ApJS*, 153, 269
- Kaplan, D. L., Kulkarni, S. R., & van Kerkwijk, M. H. 2002a, *ApJ*, 579, L29
- 2003a, *ApJ*, 588, L33
- Kaplan, D. L., Kulkarni, S. R., van Kerkwijk, M. H., & Marshall, H. L. 2002b, *ApJ*, 570, L79
- Kaplan, D. L. & van Kerkwijk, M. H. 2005a, *ApJ*, 628, L45
- 2005b, *ApJ*, 635, L65
- 2009, *ApJ*, 692, L62
- Kaplan, D. L., van Kerkwijk, M. H., & Anderson, J. 2002c, *ApJ*, 571, 447
- 2007, *ApJ*, 660, 1428
- Kaplan, D. L. et al. 2003b, *ApJ*, 590, 1008
- Kaspi, V. M. & McLaughlin, M. A. 2005, *ApJ*, 618, L41
- Kondratiev, V. I., McLaughlin, M. A., Lorimer, D. R., Burgay, M., Possenti, A., Turolla, R., Popov, S. B., & Zane, S. 2009, *ApJ*, 702, 692
- Kramer, M. 2008, AIPC, 983, 11
- Kramer, M., Lyne, A. G., Hobbs, G., Löhmer, O., Carr, P., Jordan, C., & Wolszczan, A. 2003a, *ApJ*, 593, L31
- Kramer, M., Lyne, A. G., O'Brien, J. T., Jordan, C. A., & Lorimer, D. R. 2006, *Science*, 312, 549
- Kramer, M. et al. 2003b, *MNRAS*, 342, 1299
- Kumar, H. S. & Safi-Harb, S. 2008, *ApJ*, 678, L43
- Lai, D. 2001, in *Lecture Notes in Physics*, Vol. 578, *Physics of Neutron Star Interiors*, ed. D. Blaschke, N. K. Glendenning, & A. Sedrakian (Berlin: Springer Verlag), 424
- Leahy, D. A., Tian, W., & Wang, Q. D. 2008, *AJ*, 136, 1477
- Leahy, D. A. & Tian, W. W. 2008, *A&A*, 480, L25
- Li, X. H., Lu, F. J., & Li, T. P. 2005, *ApJ*, 628, 931
- Lorimer, D. R. & Kramer, M. 2004, *Handbook of Pulsar Astronomy* (Cambridge, UK: Cambridge University Press)
- Lu, F. J., Wang, Q. D., Aschenbach, B., Durouchoux, P., & Song, L. M. 2002, *ApJ*, 568, L49
- Lutz, T. E. & Kelker, D. H. 1973, *PASP*, 85, 573
- Lyne, A. G., Pritchard, R. S., & Graham-Smith, F. 1993, *MNRAS*, 265, 1003
- Manchester, R. N., Hobbs, G. B., Teoh, A., & Hobbs, M. 2005, *AJ*, 129, 1993
- Marshall, H. L. & Schulz, N. S. 2002, *ApJ*, 574, 377
- McLaughlin, M. A., et al. 2007, *ApJ*, 670, 1307
- McLaughlin, M. A. et al. 2006, *Nature*, 439, 817
- Medin, Z. & Lai, D. 2007, *MNRAS*, submitted
- Migliazzo, J. M., Gaensler, B. M., Backer, D. C., Stappers, B. W., van der Swaluw, E., & Strom, R. G. 2002, *ApJ*, 567, L141
- Misanovic, Z., Pavlov, G. G., & Garmire, G. P. 2008, *ApJ*, 685, 1129
- Motch, C., Pires, A. M., Haberl, F., Schwope, A., & Zavlin, V. E. 2009, *A&A*, 497, 423
- Motch, C., Zavlin, V. E., & Haberl, F. 2003, *A&A*, 408, 323
- Motch, C. et al. 2005, *A&A*, 429, 257
- Ng, C.-Y., Romani, R. W., Brisken, W. F., Chatterjee, S., & Kramer, M. 2007, *ApJ*, 654, 487
- Page, D., Lattimer, J. M., Prakash, M., & Steiner, A. W. 2004, *ApJS*, 155, 623
- Pavlov, G. G. & Panov, A. N. 1976, *Soviet Phys. JETP*, 44, 300
- Pavlov, G. G., Zavlin, V. E., Sanwal, D., Burwitz, V., & Garmire, G. P. 2001, *ApJ*, 552, L129
- Pons, J. A., Miralles, J. A., & Geppert, U. 2009, *A&A*, 496, 207
- Popov, S. B., Colpi, M., Prokhorov, M. E., Treves, A., & Turolla, R. 2000a, *ApJ*, 544, L53

- . 2003, *A&A*, 406, 111
- Popov, S. B., Colpi, M., Treves, A., Turolla, R., Lipunov, V. M., & Prokhorov, M. E. 2000b, *ApJ*, 530, 896
- Popov, S. B., Posselt, B., Haberl, F., Trümper, J., Turolla, R., & Neuhäuser, R. 2008, *AIPC*, 983, 357
- Popov, S. B., Turolla, R., & Possenti, A. 2006, *MNRAS*, 369, L23
- Posselt, B. et al. 2007, *Ap&SS*, 308, 171
- Possenti, A., Cerutti, R., Colpi, M., & Mereghetti, S. 2002, *A&A*, 387, 993
- Ransom, S. M., Eikenberry, S. S., & Middleditch, J. 2002, *AJ*, 124, 1788
- Rea, N., et al. 2009, *ApJ*, 703, L41
- Rea, N. et al. 2007, *MNRAS*, 379, 1484
- Romani, R. W. & Ng, C.-Y. 2003, *ApJ*, 585, L41
- Safi-Harb, S. & Kumar, H. S. 2008, *ApJ*, 684, 532
- Schwope, A. D., Hambaryan, V., Haberl, F., & Motch, C. 2005, *A&A*, 441, 597
- . 2007, *Ap&SS*, 308, 619
- Smith, H. 2003, *MNRAS*, 338, 891
- van Kerkwijk, M. H. & Kaplan, D. L. 2007, *Ap&SS*, 308, 191
- . 2008, *ApJ*, 673, L163
- van Kerkwijk, M. H., Kaplan, D. L., Durant, M., Kulkarni, S. R., & Paerels, F. 2004, *ApJ*, 608, 432
- van Kerkwijk, M. H., Kaplan, D. L., Pavlov, G. G., & Mori, K. 2007, *ApJ*, 659, L149
- van Kerkwijk, M. H. & Kulkarni, S. R. 2001, *A&A*, 380, 221
- Vink, J., de Vries, C. P., Méndez, M., & Verbunt, F. 2004, *ApJ*, 609, L75
- Vranesevic, N. et al. 2004, *ApJ*, 617, L139
- Walter, F. M. 2001, *ApJ*, 549, 433
- Willingale, R., Aschenbach, B., Griffiths, R. G., Sembay, S., Warwick, R. S., Becker, W., Abbey, A. F., & Bonnet-Bidaud, J.-M. 2001, *A&A*, 365, L212
- Woods, P. M. & Thompson, C. 2006, in *Compact stellar X-ray sources*, ed. W. Lewin & M. van der Klis (Cambridge, UK: Cambridge University Press), 547
- Zampieri, L. et al. 2001, *A&A*, 378, L5
- Zane, S., de Luca, A., Mignani, R. P., & Turolla, R. 2006, *A&A*, 457, 619
- Zane, S., Mignani, R. P., Turolla, R., Treves, A., Haberl, F., Motch, C., Zampieri, L., & Cropper, M. 2008, *ApJ*, 682, 487
- Zane, S. & Turolla, R. 2006, *MNRAS*, 366, 727
- Zane, S., Turolla, R., & Drake, J. J. 2004, *Adv. Space Research*, 33, 531
- Zane, S. et al. 2002, *MNRAS*, 334, 345
- . 2005, *ApJ*, 627, 397
- Zhang, B., Sanwal, D., & Pavlov, G. G. 2005, *ApJ*, 624, L109